Catalysis Today 266 (2016) 2–8

Contents lists available at ScienceDirect

Catalysis Today

journal homepage: www.elsevier.com/locate/cattod

# Renewable hydrogen harvest process by hydrazine as scavenging electron donor using gold $TiO_2$ photocatalysts

Mariana Hinojosa-Reyes[a,*], Agileo Hernández-Gordillo[b], Rodolfo Zanella[c], Vicente Rodríguez-González[a,*]

[a] División de Materiales Avanzados, IPICYT, Instituto Potosino de Investigación Científica y Tecnológica, Camino a la Presa San José 2055, Col. Lomas 4a. sección C.P., 78216 San Luis Potosí, SLP, Mexico
[b] Instituto de Investigaciones en Materiales, Universidad Nacional Autónoma de México, Circuito Exterior SN, Ciudad Universitaria, Cátedras-CONACYT, CP 04510 Coyoacán, México D.F., Mexico
[c] Centro de Ciencias Aplicadas y Desarrollo Tecnológico, Universidad Nacional Autónoma de México, Circuito Exterior S/N, Ciudad Universitaria, A. P. 70-186, CP 04510 Coyoacán, México D.F., Mexico

ARTICLE INFO

*Article history:*
Received 7 May 2015
Received in revised form
26 September 2015
Accepted 12 October 2015
Available online 27 October 2015

ABSTRACT

The photocatalytic activity of well-known gold photocatalysts is investigated in the water splitting reaction by using either the ethanol or the hydrazine molecule as a scavenging agent in order to generate a renewable hydrogen harvest process. Gold photocatalysts are prepared by the deposition–precipitation method on sol–gel $TiO_2$ and using P25 as reference. These photocatalysts are surface and structurally characterized by $N_2$ physisorption, UV–vis and XPS spectroscopies, X-ray diffraction, $H_2$-TPR, and STEM-HAADF microscopy. The Au/$TiO_2$ photocatalysts exhibit the highest $H_2$ generation in the presence of either a high concentration of ethanol (3.5 M) or a low hydrazine concentration (20 mM). Stability tests for the Au/$TiO_2$ photocatalysts are carried out in several cycles using the same water–hydrazine solution, showing a hydrogen production enhancement followed by a steady state reaction. The stability of the production process is corroborated by both photocatalysts and the scavenging solution, which suggest either a slow concentration decrement or a dosage process of the hydrazine molecule. Hydrazine acts as a scavenging dosing agent which maintains the stability of the more photoactive catalysts for 50 h.Keywords: Gold $TiO_2$; Water splitting; Water–hydrazine; Hydrogen production



## 1. Introduction

Hydrogen is considered as an attractive alternative energy source due to the depletion of fossil fuel reserves and pollution caused by their use in combustion processes [1–3]. Currently, hydrogen is mainly obtained by using either nonrenewable resources or high-energy consumption processes which are neither environmentally friendly nor financially viable [4]. Therefore, there is great interest in the development of sustainable and economic methods for the production of hydrogen. Since the first report on the photoelectrochemical splitting of water on a $TiO_2$ electrode by Fujishima and Honda [5], water photocatalytic splitting has become a promising way for a clean, low-cost, and environment-friendly production of hydrogen by using light energy.

The efficiency of this reaction for $H_2$ production is improved when organic molecules are used as sacrificial reagents; in this case, the ethanol molecule has been extensively used as a hole scavenger [6]. Moreover, numerous organic compounds such as glycerol [7], lactic acid [8], ethanolamines [9,10], oxalic acid [11], chloroacetic acids [12], glucose [13,14], among others, have evolved from the water photocatalytic splitting process. As for the hole scavenger molecules, they have been evaluated to contribute to both the generation of a clean and simple system for hydrogen production, and the solution of global energy and environmental issues in the future. On the other hand, hydrazine can also act as an inorganic electron donor, reducing protons and producing $H_2$ thermodynamically [15]; it can also react until obtaining $NH_3$, $N_2$ and $H_2$ formation by photocatalytic decomposition using metallic nanoparticles as photocatalysts [15–17]. However, hydrazine dosed in aqueous solution has not been explored yet as a stable hole scavenger in water photocatalytic splitting by using either bare or $TiO_2$ modified with gold nanoparticles.

Although $TiO_2$ is an exceptional semiconductor due to the fact that it is environmentally friendly, non-toxic, cheap, and exhibits a long thermal stability against photo and chemical corrosion, it is not very promising due to the high recombination rate of

* Corresponding authors. Tel.: +52 44483 42000x6257.
*E-mail address:* kittyhinojosa@hotmail.com (M. Hinojosa-Reyes).

http://dx.doi.org/10.1016/j.cattod.2015.10.002
0920-5861/

photogenerated electron-hole pairs [18,19]. In order to diminish this rate, many strategies have been proposed to modify the $TiO_2$ surface by depositing noble metals [20]. Since gold is a noble metal that does not undergo corrosion under photocatalytic conditions, it can be strongly anchored as nanoparticles on the titania surface and exhibits a characteristic surface plasmon band in the visible region [21]. Despite the numerous reports dealing with the photocatalytic activity of doped and undoped $TiO_2$ as well as the thermal catalytic activity of $Au/TiO_2$, the number of reports on the photocatalytic hydrogen activity of $Au/TiO_2$ is still scarce; in this sense, it is of interest to expand the use of $Au/TiO_2$ as a photocatalyst [22].

In this work, the photocatalytic activity of $Au/TiO_2$ was evaluated in the $H_2$ production reaction. The effect of hydrazine, dosed at low concentrations as a hole scavenger in aqueous solution during the water splitting reaction, was studied for the first time in comparison with the ethanol molecule. The stabilities of the studied photocatalysts and the corresponding solutions were evaluated. In spite of hydrazine toxicity, in this work, its use as a scavenging electron donor is demonstrated. In addition, the possible interactions between the catalysts and the sacrificial reagents and the possible pathway of $H_2$ production are discussed.

## 2. Materials and methods

### 2.1. Synthesis of sol–gel photocatalysts

Sol–gel $TiO_2$ photocatalysts were prepared by a controlled sol–gel process using titanium (IV) isopropoxide (Sigma-Aldrich 97%) as a titanium precursor, and ethanol (Le Cap Group 96%) and distilled water were used as solvents. The alkoxide/ethanol/water molar ratio was 1/3/8. According to our previously reported sol–gel synthesis [23,24], a mixture of 22.9 mL of ethanol and 18 mL of water was poured in a 4-neck-round-bottom flask (1 L). Then, 75.6 mL of titanium isopropoxide were added dropwise. Later on, the mixture solution was vigorously stirred at 50 °C until all the reagents were added. Subsequent to this operation, the solution was gradually heated up to 70 °C. The gelled product was aged for 48 h at 70 °C. The solvents and unreacted precursors were removed from the xerogel by drying it overnight under vacuum at 100 °C. Finally, the solid was thermally treated at 500 °C for 4 h at a rate of 2 °C $min^{-1}$ in static air. The samples were identified as $TiO_2$.

### 2.2. Deposition–precipitation of gold nanoparticles

The photocatalysts functionalized with gold nanoparticles, AuNPs (2 wt.%), were prepared in the absence of light since it is known that it decomposes and reduces the gold precursors. The preparation of the gold nanoparticles was performed by the deposition–precipitation method with urea (DP Urea) [25,26]. $HAuCl_4$ ($4.2 \times 10^{-3}$ M), used as a gold precursor, and urea (0.42 M) were dissolved in 49.29 mL of distilled water (pH 2.4). Then, 2 g of the supports ($TiO_2$ or P25) were added to this solution under constant stirring; thereafter, the suspension was heated at 80 °C and kept steady for 16 h. The urea decomposition led to a gradual pH rise from 2.4 to 7 [26]. After the deposition–precipitation procedure, all the samples were centrifuged, washed with water at 50 °C and then centrifuged four times and dried under vacuum at 80 °C for 2 h. Then, all the impregnated solids were thermally treated at 300 °C for 2 h under dry air flow (1 mL $min^{-1}$ $mg_{sample}{}^{-1}$). All the modified catalysts were stored at room temperature under vacuum in a desiccator away from light in order to prevent any alteration [27].

### 2.3. Characterization techniques

The thermally treated photocatalysts were characterized by X-ray diffraction in order to identify crystalline phases using a Bruker Advance 8 Diffractometer with Cu$K\alpha$ radiation (1.5404 Å). Diffuse reflectance UV–vis spectra of the photocatalysts were obtained using a Cary 5000 (UV–vis–NIR) spectrophotometer; a teflon spectrum (from Agilent) was used as a reference blank and the band gap energy was determined by using the Kubelka–Munk method. The specific surface area was determined by the Brunauer–Emmett–Teller method (BET method) on a Quantachrome Autosorb 1. The hydrogen temperature programmed reduction ($H_2$-TPR) study of the dried photocatalysts was performed in a RIG-150 unit under a flow of 10% $H_2$/Ar gas mixture (30 mL $min^{-1}$) with a heating rate of 10 °C $min^{-1}$ from room temperature to 200 °C. $H_2O$ produced during the reduction process was trapped before the TCD detector. The photocatalysts were examined by transmission electron microscopy in a Tecnai FEI 300 transmission electron microscope (TEM) operated at 300 kV. The particle size distribution histograms for the photocatalysts were developed from the measurements of about 200 particles. The average particle diameter ($d_s$) was calculated using the following formula: $d_s = \sum n_i d_i / \sum n_i$, where $n_i$ is the number of particles of diameter $d_i$. X-ray photoelectron spectroscopic (XPS) technique was carried out in *K*-Alpha spectrometer by Thermo Scientific using monocromatic radiation $K\alpha$ of Al at 1486.68 eV.

### 2.4. Water splitting test

The photocatalytic activity of the gold-$TiO_2$ materials was evaluated in a home-made cylindrical glass reactor with an inner quartz tube equipped with a UV pen ray Hg lamp ($\lambda$ = 254 nm, $I_0$ = 4400 μW $cm^{-2}$). This glass reactor had a full operation volume of 250 mL and the scavenger solutions consisted of either water–ethanol (100:100 mL, 50 vol.% of $H_2O$) or water–hydrazine hydrate (199.5:0.5 mL, 99.93 vol.% of $H_2O$). Ethanol was purchased from Le Cap Group (96%) and hydrazine hydrate from Fluka (24–26%). In all the experiments, 50 mg of photocatalyst powder were used and the suspension was stirred for 20 min, while it was purged with nitrogen to remove the dissolved oxygen from the solution. After oxygen was removed, the reactor system was sealed and the UV lamp was turned on. Hydrogen determination was done every hour for 8 h in a gas chromatograph by Thermo Scientific with thermal conductivity detector and packed column by Thermo Scientific TracePLOT TG-BOND Msieve 5A. The system was calibrated previously in order to quantify the hydrogen production.

To determine the optimal hydrazine concentration, experiment runs were carried out with 30 mg of $ZnS(en)_{0.5}$ hybrid photocatalyst, varying the volume of hydrazine hydrate from 0.1 to 5 mL (4 to 203 mM) (see Supplementary section, Fig. S1). The $ZnS(en)_{0.5}$ hybrid photocatalyst is well known for its high activity in the hydrogen production by water photocatalytic splitting [28,29]. Additionally, a photocatalytic test was carried out only with water in order to get more insights about the drive-hydrazine water splitting.

For the stability test, four cycles of 8 h each were carried out for the selected active photocatalyst ($Au/TiO_2$). After running the experiments, the UV lamp was turned off, the produced hydrogen was released and the reaction system was purged with nitrogen until the chromatographic hydrogen signal was zero. Then, the reactor system was sealed and the lamp was turned on again to start the next cycle and so on until the fourth cycle was completed. At the same time, hydrazine evolution was measured by sampling aliquots every 30 h and then they were analyzed by UV–vis

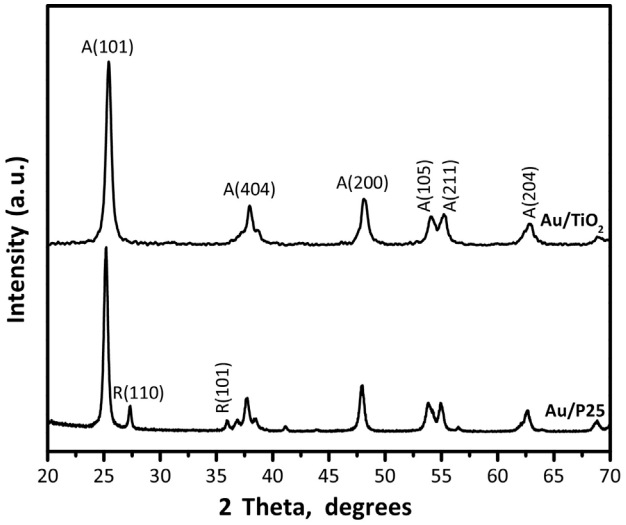


**Fig. 1.** X-ray diffraction patterns of the $Au/TiO_2$ and Au/P25 photocatalysts.

**Table 1**
Band-gap energy, crystallite size, specific surface area, and AuNP size for $Au/TiO_2$ and Au/P25 photocatalysts.

| | $E_g$ (eV) | Crystallite size (nm) | Surface area ($m^2\ g^{-1}$) | AuNP size (nm) |
|---|---|---|---|---|
| $Au/TiO_2$ | 2.99 | 16.3 | 72.7 | 3.0 |
| Au/P25 | 3.20 | 19.7 | 51.3 | 3.4 |

spectroscopy following the band that occurred at 210 nm, according to the hydrazine calibration curve, Fig. S2.

## 3. Results and discussion

### 3.1. Characterization of photocatalysts

The XRD patterns for all the gold photocatalysts, Fig. 1, indicate the presence of the anatase crystalline phase for $Au/TiO_2$ (JCPDS 04-002-2678), whereas for the bare commercial Au/P25, the presence of the rutile crystalline phase was also observed (JCPDS 04-014-1641). As for the diffraction peaks associated with metallic $Au^0$, no $Au^{3+}$ oxides were detected due to the low concentration of these gold nanoparticles.

Through full width at half-maximum (FWHM) of the (1 0 1) anatase peak at $2\theta = 25.2^\circ$, the crystallite size was calculated using the Scherrer equation [30]. A slightly smaller crystallite size of the sol–gel $TiO_2$ was detected with respect to the commercial P25 (Table 1), which was probably due to the effect of the synthesis method.

The specific surface areas for both gold photocatalysts are shown in Table 1, which indicates that the sol–gel $TiO_2$ photocatalyst presents higher specific surface area with respect to the commercial P25. These results show a correlation between the crystallite size and the surface area: the smaller the crystallite size, the higher the surface area. Thereby, the sol–gel method is responsible for providing a photocatalyst with this enhanced surface property.

UV–vis spectra for the sol–gel $TiO_2$ support and both gold photocatalysts are shown in Fig. 2, and from these spectra, the band gap ($E_g$, Table 1) was estimated through the extrapolation of the linear portion of the $(FR \times h\nu)^{1/2}$ vs $h\nu$ curves to FR = 0 [31]. The direct transition was selected because the indirect transitions can occur simultaneously with direct transitions, but they cannot be detected in the absorption spectrum due to their high energy and low probability [31].

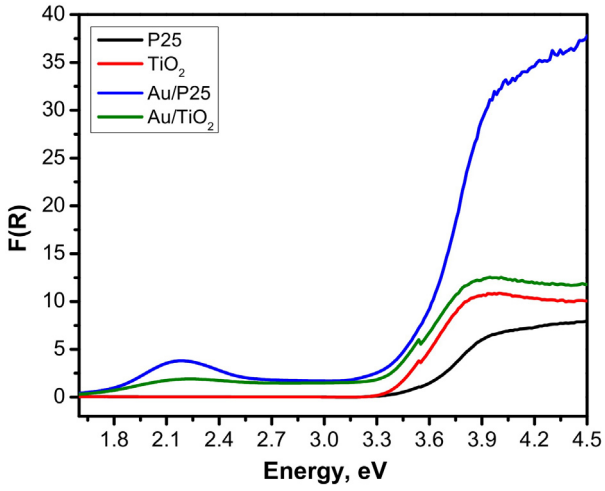


**Fig. 2.** Kubelka–Munk plot of the $Au/TiO_2$ and Au/P25 photocatalysts.

The $TiO_2$ and P25 supports show $E_g$ values of 3.22 and 3.26 eV, respectively. The incorporation of AuNPs exerts an electronic effect that decreases the band gap value. In addition, the surface plasmon resonance (SPR), considered as the collective oscillation of electrons by incident light, occurred at around 550 nm (2.2 eV) for the AuNPs, which is observed for both $Au/TiO_2$ and Au/P25 photocatalysts.

Transmission electron microscopy images in the STEM-HAADF mode are shown in Fig. 3. In all the cases, a homogeneous dispersion of the AuNPs over the $TiO_2$ and P25 supports was found. According to the frequency histogram for each photocatalyst, AuNPs with size distributions ranging from 3.0 to 3.4 nm are found, and for Au/P25, larger AuNPs sizes are observed (up to 4 nm). Thus, DPU is a good technique for depositing AuNPs over metallic oxides. Due to the low gold loading and high dispersion, and as consequence, to small particle sizes, no diffraction peak was detected by XRD.

Temperature programmed reduction data of the fresh gold photocatalysts are shown in Fig. 4. In the sol–gel $Au/TiO_2$ and Au/P25 samples, a peak that starts at 120 °C and ends at 165 °C with maxima at 142 and 145 °C is observed, respectively. These maxima indicate the temperature reduction from $Au^{3+}$ to $Au^0$ and stem from the reduction of Au(III) species from the gold precursor $HAuCl_4$ [32,33]. It is also remarkable that for similar AuNP sizes, these samples have slightly different gold reduction temperatures. In addition, the P25 sample was also analyzed by this technique, and no reduction peaks were detected, corroborating that the peak at around 120–165 °C belongs to the reduction of the $Au^{3+}$ to $Au^0$ species, [34], as it can be contrasted in Fig. 4. Also, at higher temperatures, the $Ti^{4+}$ support reduction is observed, emphasizing that $Au/TiO_2$ support has a maximum peak at 370 °C, while Au/P25 it has at 454 °C, This difference in temperatures indicates that gold deposition play an interesting role during the reduction process of the catalysis, enhancing the $Au/TiO_2$ photoactivity during the $H_2$ water-splitting production due to a strong metal interaction and as a consequence to the high electron transference.

The XPS analysis confirmed the oxidation state of the AuNPS, Fig. 5. Gold shows two 4f bands, where their deconvolution shows that most gold is in a reduced state (88 and 84 eV) and there is also $Au^{3+}$ (94 and 87 eV) which is associated with the interface between AuNPs and $TiO_2$ [35,36].

### 3.2. Photocatalytic test in $H_2$ production

#### 3.2.1. Using an ethanol scavenging aqueous solution

The gold photocatalysts were tested under oxidizing conditions using 50 vol.% of ethanol (3.5 M) as a hole scavenger and the results

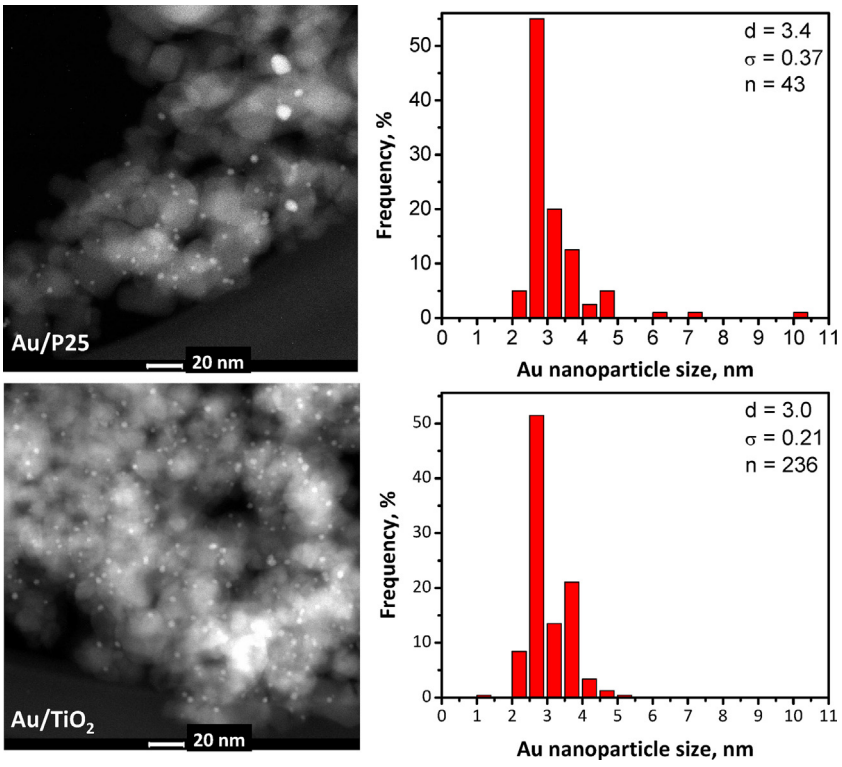


**Fig. 3.** STEM-HAADF images and size distribution histograms of the $Au/TiO_2$ and Au/P25 photocatalysts.

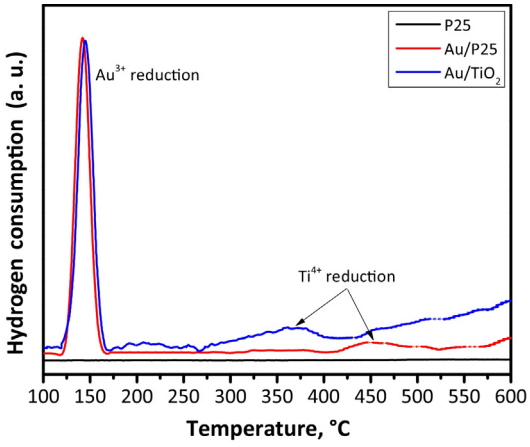


**Fig. 4.** TPR thermograms of fresh $Au/TiO_2$ and Au/P25, and P25 photocatalysts.

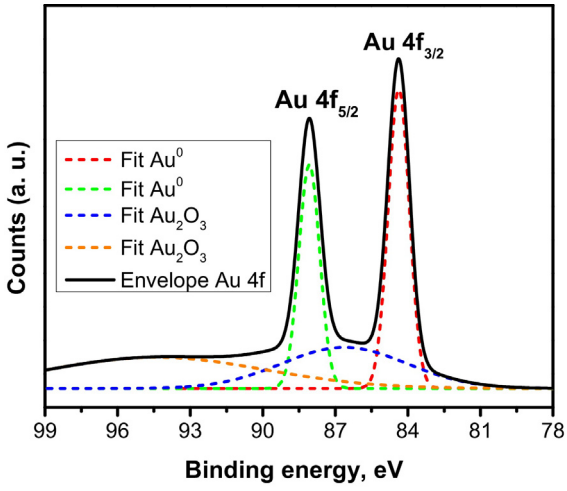


**Fig. 5.** Deconvolutionated XPS spectra of Au 4f orbital of $Au/TiO_2$ (300 °C/Air).

are shown in Fig. 6. The $H_2$ production was standardized as a function of time of the run test ($\mu mol\,h^{-1}$), where for all the samples, the photolysis value was subtracted. It was observed immediately that the sol–gel $Au/TiO_2$ photocatalyst featured the best hydrogen production (368 $\mu mol\,h^{-1}$), almost 7 times higher with respect to photolysis (see Table 2), and even 4 times more active than Au/P25. These hydrogen production values are higher than those reported in the literature [18,19].

This behavior can be associated with the interactions between the AuNPs and the sol–gel $TiO_2$ and with the particle size that is smaller than that of commercial P25. It could also be associated with the high surface hydroxyl coverage; therefore, the influence of titanol groups (TiOH) from the $TiO_2$ surface, caused by the air thermal treatment, is well known because they are important trapping centers for the valence-band holes, which are the principal oxidizing sites on the $TiO_2$ surface [37].

**Table 2**
Comparative chart about hydrogen production.

| | $H_2$ production ($\mu mol\,h^{-1}$) | |
|---|---|---|
| | Water–ethanol (*n* times)* | Water–hydrazine (*n* times)* |
| Photolysis | 54.4 | 10.1 |
| $TiO_2$ | 55.7 (1.0) | 13.1 (1.3) |
| P25 | 61.2 (1.1) | 8.4 (0.8) |
| $Au/TiO_2$ | 368.2 (6.8) | 48.5 (4.8) |
| Au/P25 | 88.3 (1.6) | 17.0 (1.7) |

* *n* times with respect to photolysis.

Therefore, an important difference between photocatalysts is the presence of the rutile phase in the P25 photocatalyst. By considering that the band gap energy of anatase is 3.2 eV and that that of rutile is 3.0 eV, it can be said that the crystal structure

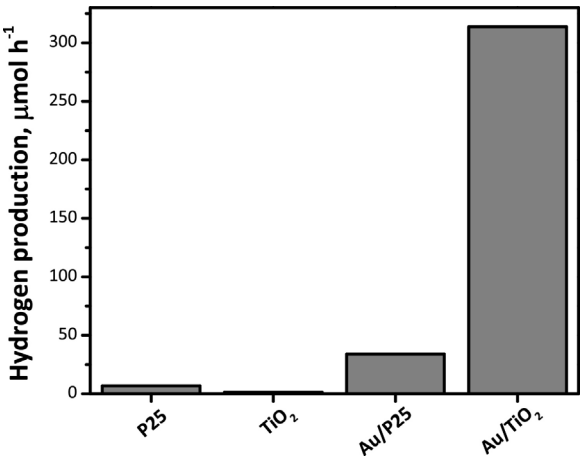


**Fig. 6.** Standardized $H_2$ production with 0.05 g of the supports and gold photocatalysts using a water–ethanol solution (50 vol.%, 3.5 M).

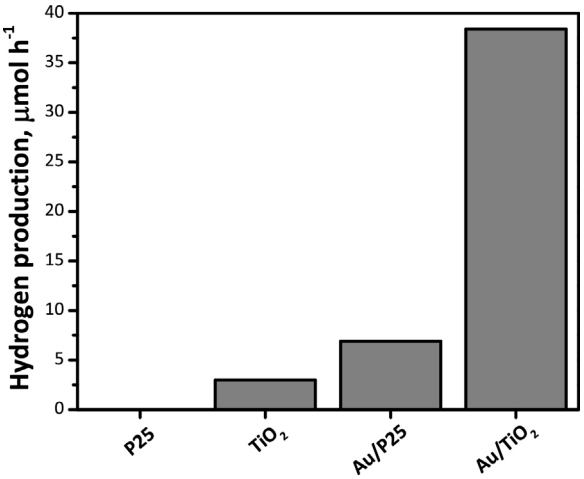


**Fig. 7.** Standardized $H_2$ production with 0.05 g of the supports and gold photocatalysts using a water–hydrazine solution (0.25 vol.%, 20 mM).

determines the band gap energy, suggesting that the conduction band level of anatase is higher than that of rutile [38]. Therefore, the phase combination between anatase and rutile might be the cause of the low photocatalytic activity [6]. By taking into account that the water splitting reaction takes place at the conduction band, the anatase highly crystalline phase has the necessary energy to conduct the electron transfer process more efficiently and reduce the $H^+/H_2$ couple with respect to NHE.

In contrast, the use of the nanocrystalline mesoporous $TiO_2$ with high crystallinity could decrease the number of lattice defects, also avoiding the $h^+/e^-$ recombination, and then making the electron transport easier for reacting with water molecules adsorbed on the $TiO_2$ surface [39].

The anatase phase has a density of surface hydroxyl groups that is higher than that of rutile, the anatase/rutile ratio (80/20 for P25), which plays an important role [40].

In early studies, anatase $TiO_2$ was believed to be a more efficient photocatalyst than rutile $TiO_2$ due to its higher Fermi level and higher hydroxylation degree. For example, Verykios and Karakitsou reported that hydrogen photocatalytic production from water splitting over platinized $TiO_2$ was significantly affected by the crystalline structure of $TiO_2$ and that the anatase phase exhibited several times higher hydrogen production rates than rutile [41].

The evaluation of the supports is also important because it is known that either bare $TiO_2$ or P25 are not quite effective to achieve hydrogen production. According to these results, the $H_2$ production was discreet using both bare $TiO_2$ (55.7 $\mu$mol $h^{-1}$) or commercial P25 (61.2 $\mu$mol $h^{-1}$), which helped corroborate that AuNPs act as electron traps that prevent charge recombination [22].

### 3.2.2. *Hydrazine hydrate in water as a dosed scavenging agent*

A hydrazine scavenging system, as a novel hydrogen production method, was explored by using an aqueous solution dosed with 0.5 mL of hydrazine, which was used as a hole scavenger. In this case, the optimal hydrazine concentration for hydrogen production was determined by using the $ZnS(en)_{0.5}$ photocatalyst (see Supplementary section, Fig. S1) and it was found that a dose of 0.5 mL of hydrazine hydrate (20 mM) showed an overall hydrogen production of 70 $\mu$mol $h^{-1}$, and when 1 mL of hydrazine (40 mM) was used, a slight increase in the hydrogen production (80 $\mu$mol $h^{-1}$) was observed, which is considered as a steady-state process. This steady-state condition suggests that hydrogen evolution is provided by water.

So, this experiment series of hydrogen production was performed in the absence of photocatalyst (photolysis), and the result was used as a reference (10.1 $\mu$mol $h^{-1}$). Photolysis experiments assure that the produced hydrogen comes from water splitting and not from a scavenging agent. The photocatalytic evaluation of the Au photocatalysts was carried out with 0.5 mL of hydrazine (optimal concentration), see Fig. 7.

The test regarding the support evaluation indicated that only the sol–gel $TiO_2$ support presented hydrogen photocatalytic evolution (13.1 $\mu$mol $h^{-1}$), 1.3 times higher than that of photolysis. As for commercial P25, the hydrogen production was negligible (8.4 $\mu$mol $h^{-1}$). When the supports were functionalized with AuNPs, they exhibited better hydrogen production than that obtained by photolysis, but the sol–gel $Au/TiO_2$ was the best photocatalyst with an overall production of 48.5 $\mu$mol $h^{-1}$, which was 4.8 times higher than that coming from photolysis (Table 2). In this case, the amount of generated hydrogen (38.4 $\mu$mol $h^{-1}$) is not comparable with that generated with the water–ethanol system (313.8 $\mu$mol $h^{-1}$) because the hydrazine amount was extremely low, however, despite the low dose (20 mM), the $H_2$ production was high and stable.

With this hole scavenger, also, the $Au/TiO_2$ results to be the most active due probably to the fact that the electronic transfer of the anatase crystalline phase is more efficient in the sol–gel $TiO_2$.

A blank experiment without scavenger agent using $Au/TiO_2$ as photocatalyst indicated a non-negligible hydrogen production of 15.8 $\mu$mol $h^{-1}$, which corroborated that hydrazine improves considerably the hydrogen production. A second cycle only achieved a hydrogen production of 11.7 $\mu$mol $h^{-1}$, which means that the hydrazine system also acts as a stable dosage scavenging system, see Supplementary section, Fig. S3. To elucidate the hydrazine decomposition, another blank experiment was carried out in dark conditions, first with 0.05 mL of hydrazine scavenger and no hydrogen production was detected. Even with a five times more of hydrazine concentration any hydrogen production was detected.

According to these results, the photocatalytic production of $H_2$ is enhanced according to the used hole scavenger and it can be assumed that the sol–gel method provides small $TiO_2$ crystals and the AuNP functionalization also helps to reduce the recombination rate. Furthermore, gold provides electronic stability in the involved redox reactions. Synergic effects coming from the air thermal treatment and light absorbance of the AuNPs also contribute to enhance the hydrogen production in this water–hydrazine system. These hydrogen production results indicate higher production and more stability for both photocatalysts and solution systems in comparison with the $NaBH_4$ hole scavenger, which is well known for its hydrogen evolution from hydrolysis [42]. The use of hydrazine as a dosage scavenging agent enhances the water splitting and

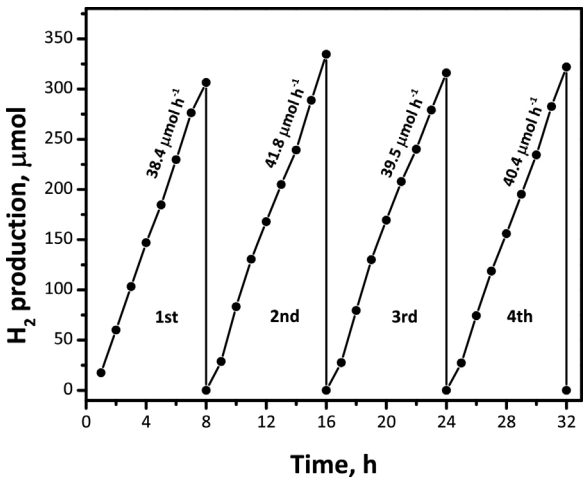


**Fig. 8.** $H_2$ production profiles for the four reaction cycles with Au/$TiO_2$ using the same water–hydrazine solution.

preserves the activity for more than 4 cycles with negligible deactivation.

Table 2 is a summary of hydrogen produced by the different photocatalysts (supports and gold photocatalysts); it serves as a comparative chart to elucidate the most active photocatalysts during the water splitting reactions.

### 3.2.3. *Stability test*

A stability test run was carried out in the water–hydrazine system by using the Au/$TiO_2$ photocatalyst, see Fig. 8, which showed a similar hydrogen production (40 µmol $h^{-1}$) for four cycles equivalent to one and a half days without any deactivation using the same water–hydrazine solution. These results suggest that the AuNPs are stable on the $TiO_2$ photocatalyst and that the low hydrazine concentration is still scavenging the water splitting reaction with a continuous hydrogen production for at least 32 h.

During the stability test, the hydrazine evolution indicated a constant depletion rate of an electron donor molecule (hydrazine) even at low hydrazine dosing. So, the hydrazine evolution decreased at around 74% after 32 h of reaction with constant hydrogen production, Fig. 9, which indicates that hydrazine can act as a scavenger agent at very low concentrations, and drive the hydrogen production from water.

A new absorption band from 220 to 340 nm (Fig. 9) was associated with the intermediary formation [43]. After 48 h of photocatalytic reaction, hydrazine was almost consumed (91%) and the absorption band of the intermediaries was also decreased with an almost negligible $H_2$ production rate (0.45 µmol $h^{-1}$), indicating that a minimum concentration of hydrazine (up 4.4 mM) is necessary to achieve high $H_2$ production rates.

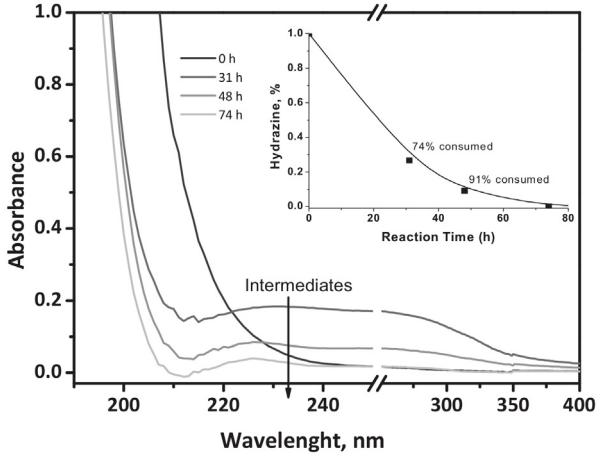


**Fig. 9.** UV–vis spectra of hydrazine evolution with respect to time using Au/$TiO_2$ as photocatalyst.

## 4. Conclusions

The sol–gel synthesis in conjunction with the AuNP deposition–precipitation method produce active water photocatalytic splitting with remarkable $H_2$ production in both water–ethanol and water–hydrazine scavenging solutions: (i) the sol–gel Au/$TiO_2$ catalyst featured the highest $H_2$ production in both scavenging systems; (ii) the presence of the rutile crystalline phase causes a decrement in the hydrogen photocatalytic production because anatase $TiO_2$ has a higher Fermi level as well as a higher hydroxylation degree; (iii) the excellent Au/$TiO_2$ photoactivity is possible due to the surface titanol groups, generated by the air thermal treatment, which are important trap centers for the valence-band holes; (iv) gold nanoparticles exert an electron trapping effect that enhances the $H_2$ production in addition to the well-known photocatalytic effect occurring in bare $TiO_2$; (v) the hole consumption pathway involves the reduction of protons over the AuNPs to hydrogen production, giving hydrazine the role of a scavenging dosing agent which maintains the stability of the highest active catalyst for 50 h; (vi) the results obtained with water dosed with hydrazine as scavenging agent are promising and efficient in the water photocatalytic splitting for $H_2$ production and give insights about how to tune positively the photoactivity by doping sol–gel $TiO_2$ with non-transition metal ions.

## Acknowledgements

M. H. R. thanks CONACYT for the Ph. D. scholarship. The use of the CCADET and LINAN infrastructures are also gratefully acknowledged. We thank V. Maturano Rojas, M. Cisneros, B. A. Rivera-Escoto and H. G. Silva Pereyra for their technical assistance. We thank SEP CONACYT-CB-2011/169597, Infra-2014/225945 and CB-2009 130407 projects and DGAPA-PAPIIT (Project 103513) for the provided financial support.

## Appendix A. Supplementary data

Supplementary data associated with this article can be found, in the online version, at http://dx.doi.org/10.1016/j.cattod.2015.10.002.

## References

[1] R.D. Cortright, R.R. Davda, J.A. Dumesic, Nature 418 (2002) 964–967.
[2] S. Abanades, P. Charvin, G. Flamant, P. Neveu, Energy 31 (2006) 2805–2822.
[3] S. Abanades, G. Flamant, Sol. Energy 80 (2006) 1611–1623.
[4] J.A. Turner, Science 305 (2004) 972–974.
[5] A. Fujishima, K. Honda, Nature 238 (1972) 37–38.
[6] A. Kudo, Y. Miseki, Chem. Soc. Rev. 38 (2009) 253–258.
[7] V.M. Daskalaki, P. Panagiotopoulou, D.I. Kondarides, Chem. Eng. J. 170 (2011) 433–439.
[8] W. Zhang, Y. Wang, Z. Wang, Z. Zhong, X. Ru, Chem. Commun. 46 (2010) 7631.
[9] A.J. Bard, M.A. Fox, Acc. Chem. Res. 28 (1995) 141–145.
[10] Y. Li, K. Zhang, S. Peng, G. Lu, S. Li, J. Mol. Catal. A: Chem. 363–364 (2012) 354–361.
[11] Y. Li, G. Ju, S. Li, Appl. Catal. A: Gen 214 (2001) 179–185.
[12] Y. Li, Y. Xie, S. Peng, G. Lu, S. Li, Chemosphere 63 (2006) 1312–1318.
[13] Y. Li, J. Wang, S. Peng, G. Lu, S. Li, Int. J. Hydrogen Energy 35 (2010) 7116–7126.
[14] Y. Li, D. Gao, S. Peng, G. Lu, S. Li, Int. J. Hydrogen Energy 36 (2011) 4291–4297.
[15] Y. Oosawa, J. Chem. Soc., Faraday Trans. 80 (1984) 1507–1515.
[16] T. Abe, N. Taira, Y. Tanno, Y. Kikuchia, K. Nagaib, Chem. Commun. 50 (2014) 1950–1952.
[17] H. Yuzawa, T. Mori, H. Itoh, H. Yoshida, J. Phys. Chem. C 116 (2012) 4126–4136.
[18] M. Ni, M.K.H. Leung, D.Y.C. Leung, K. Sumathy, Renewable Sustainable Energy Rev. 11 (2007) 401–425.

[19] J. Yu, L. Qi, M. Jaroniec, J. Phys. Chem. C 114 (2010) 13118–13125.
[20] T. Srethawong, S. Yoshikawa, Catal. Commun. 6 (2005) 661–668.
[21] C.J. Orendorff, T.K. Sau, C.J. Murphy, Small 2 (2006) 636–639.
[22] C. Gomes Silva, R. Juárez, T. Marino, R. Molinari, H. García, J. Am. Chem. Soc. 133 (2011) 595–602.
[23] V. Rodríguez-González, A. Moreno-Rodríguez, M. May, F. Tzompantzi, R. Gómez, J. Photochem. Photobiol., A: Chem. 193 (2008) 266–270.
[24] V. Rodríguez-González, F. Paraguay-Delgado, X. García-Montelongo, L.M. Torres-Martínez, R. Gómez, J. Ceram. Process. Res. 9 (2008) 606–610.
[25] R. Zanella, S. Giorgio, C.R. Henry, C. Louis, J. Phys. Chem. B 106 (2002) 7634–7642.
[26] R. Zanella, L. Delannoy, C. Louis, Appl. Catal. A: Gen 291 (2005) 62–72.
[27] R. Zanella, C. Louis, Catal. Today 107 (2005) 768–777.
[28] A. Hernández Gordillo, F. Tzompantzi, R. Gómez, Int. J. Hydrogen Energy 37 (2012) 17002–17008.
[29] A. Hernández-Gordillo, F. Tzompantzi, R. Gómez, Catal. Commun. 19 (2012) 51–55.
[30] A. Guinier, X-ray Diffraction in Crystals, Imperfect Crystals and Amorphous Bodies, second ed., W. H. Freeman Company, San Francisco, CA, 1963.
[31] R. López, R. Gómez, J. Sol-Gel Sci. Technol. 61 (2012) 1–7.
[32] A. Sandoval, A. Gómez-Cortés, R. Zanella, G. Díaz, J.M. Saniger, J. Mol. Catal. A: Chem. 278 (2007) 200–208.
[33] A. Sandoval, A. Aguilar, C. Louis, A. Traverse, R. Zanella, J. Catal. 281 (2011) 40–49.
[34] A. Aguilar-Tapia, R. Zanella, C. Calers, C. Louis, L. Delannoy, Phys. Chem. Chem. Phys. (2015), http://dx.doi.org/10.1039/C5CP00590F.
[35] M.P. Casaletto, A. Longo, A. Martorana, A. Prestianni, A.M. Venezia, Surf. Interface Anal. 38 (2006) 215–218.
[36] B. Schumacher, V. Plzak, M. Kinne, R.J. Behm, Catal. Lett. 89 (2003) 109–114.
[37] N.L. Wu, M.S. Lee, Z.J. Pon, J.Z. Hsu, J. Photochem. Photobiol., A: Chem. 163 (2004) 277–280.
[38] K. Shimura, H. Yoshida, Energy Environ. Sci. 4 (2011) 2467–2481.
[39] T. Sreethawong, Y. Suzuki, S. Yoshikawa, Catal. Commun. 6 (2005) 119–124.
[40] O. Rosseler, S.V. Muthukonda, M. Karkmaz-Le Du, S. Schmidlin, N. Keller, V. Keller, J. Catal. 269 (2010) 179–190.
[41] K.E. Karakitsou, X.E. Verykios, J. Phys. Chem. 97 (1993) 1184–1189.
[42] Y. Lee, Y. Kim, H. Jeong, M. Kang, J. Ind. Eng. Chem. 14 (2008) 655–660.
[43] E. Hayon, M. Simic, J. Am. Chem. Soc. 94 (1972) 42–47.